

The Evolution of Intermolecular Energy Bands of Occupied and Unoccupied Molecular States in Organic Thin Films

Yuki Kashimoto¹, Keiichirou Yonezawa², Matthias Meissner^{2,3}, Marco Gruenewald³, Takahiro Ueba²,
Satoshi Kera^{1,2*}, Roman Forker³,
Torsten Fritz^{3*}, Hiroyuki Yoshida^{1,4*}

¹*Graduate School of Engineering, Chiba University, 1-33, Yayoi-cho, Inage-ku, Chiba 263-8522, Japan*

²*Institute for Molecular Science, Myodaiji, Okazaki, 444-8585, Japan*

³*Institut für Festkörperphysik, Friedrich-Schiller-Universität Jena, Helmholtzweg 5, 07743 Jena, Germany*

⁴*Molecular Chirality Research Center, Chiba University, 1-33, Yayoi-cho, Inage-ku, Chiba 263-8522, Japan*

Abstract

In organic semiconductors, the hole and electron transport occurs through the intermolecular overlaps of highest occupied molecular orbitals (HOMO) and lowest unoccupied molecular orbitals (LUMO), respectively. A measure of such intermolecular electronic coupling is the transfer integral, which can experimentally be observed as energy level splittings or the width of the respective energy bands. Quantum chemistry textbooks describe how an energy level splits into two levels in molecular dimers, into three levels in trimers and evolves into an energy band in infinite systems, a process that has never been observed for the LUMO or beyond dimers for the HOMO. In this work, our new technique, low-energy inverse photoelectron spectroscopy, was applied to observe the subtle change of the spectral line shape of a LUMO-derived feature while we used ultraviolet photoelectron spectroscopy to investigate the occupied states. We show at first that tin-phthalocyanine molecules grow layer-by-layer in quasi one-dimensional stacks on graphite, and then discuss a characteristic and systematic broadening of the spectral line shapes of both HOMO and LUMO. The results are interpreted as energy-level splittings due to the intermolecular electronic couplings. Based on the Hückel approximation, we determined the transfer integrals for HOMO-1, HOMO, and LUMO to be ≤ 15 meV, (100 ± 10) meV, and (128 ± 10) meV, respectively.

1. Introduction

Since the middle of the last century, the transport mechanisms in organic semiconductors have been a central and sometimes controversially discussed research topic. The charge carrier transport is determined by the intermolecular overlap of π -orbitals of the constituent molecules ¹. A good measure of the intermolecular orbital overlap is the bandwidth of the resulting bands and the transfer integral t between the orbitals involved. In the early stage of research the bandwidths of organic solids were believed to be a few tens of meV at maximum ². Since the 1990s, however, k -resolved ultraviolet photoelectron studies showed intermolecular energy band dispersions with the bandwidth exceeding 0.1 eV in organic solids ³, and later on small bandwidths less than 0.1 eV were observed⁴.

While the bandwidths can be obtained experimentally via photoelectron spectroscopies, the transfer integral t is the primary parameter for the theoretical treatment of carrier transport. In organic solids, the transfer integral is connected with the bandwidth (or the energy level splitting) in the framework of the tight-binding approximation, when the molecular orbital is taken as a basis (and not atomic orbitals, as in inorganic solids). Further, here the transfer integrals of only the nearest-neighbor molecules are taken into consideration and the overlap integrals are ignored, which is referred to as the Hückel approximation, as it is conceptually equivalent to the treatment of atomic orbitals in the Hückel LCAO (Linear Combination of Atomic Orbitals). The simplest example is a one-dimensional molecular chain. When two molecules approach each other, every energy level splits into two with an energy difference $2t$, where t will be different for the different energy levels and may even become zero. Three and four molecules generate three and four levels, respectively, and if the molecular chain length approaches infinity, the separation of energy levels becomes increasingly close until a one-dimensional band with a continuous density of states is formed as schematically shown in Figure 1 ⁵. Therefore, we will refer to our model in the following as Hückel model for short.

Although a calculated dimer splitting of $2t$ is often used to determine the transfer integral as described in the theory of organic semiconductors ¹, an experimental observation of the splitting is much more challenging than measuring the band dispersion because it requires precise control of the uniformity and the number of layers in the film, in addition to preparing a film with a desired crystal structure and molecular orientation, as the transfer integral depends rather sensitively on the

molecular alignment ⁶⁻⁷. In 2007, Kera et al. demonstrated that splitting of the highest occupied molecular orbital (HOMO) occurs in a bilayer of lead-phthalocyanine (PbPc) and derived a transfer integral of 175 meV at 295 K ⁸.

Most studies published so far focus only on the hole transport based on the intermolecular orbital interaction of HOMO-derived levels. In fact, no experimental data are available for the intermolecular orbital overlap of LUMO-derived levels. In a bipolar semiconductor device such as an organic light emitting diode or an organic photovoltaic cell, however, not only the hole but also the electron plays a central role for its performance. The intermolecular orbital interaction of the lowest unoccupied molecular orbitals (LUMO) is responsible for electron conduction. Although intermolecular orbital interaction between LUMOs is often assumed to be similar to that between HOMOs, this assumption can be challenged for the following reasons: (i) The shapes of HOMO and LUMO wavefunctions are different. For example, the number of nodes is larger in the LUMO than in the HOMO, leading to a smaller transfer integral for the LUMO. (ii) Quite oppositely, the spatial extensions are different for occupied and unoccupied molecular orbitals because a charge carrier in the LUMO (excess electron) and a hole in the HOMO (electron deficiency) may increase and reduce the shielding of the positive charge of atomic cores, respectively, leading to a LUMO transfer integral that is larger than that of the HOMO. Therefore, the LUMO's transfer integral may be larger or smaller than the HOMO's, depending on which effect is stronger, but at least it will most likely be different. Furthermore, most organic semiconductors predominantly show hole conduction, and developing a "n-type" semiconductor with high electron mobility has been a central issue in organic electronics ⁹⁻¹⁰. Therefore, understanding the electron conduction via the LUMO is both interesting and challenging at the same time.

The main reason for the non-existence of experimental data for the LUMO transfer integral is a lack of suitable experimental methods for unoccupied states of organic semiconductors. Although the optical transition from HOMO to LUMO, employing UV-vis absorption spectroscopy or two-photon photoelectron spectroscopy, is often used to estimate the LUMO-derived levels indirectly (problems may arise from the exciton binding energy which is not known in most cases ¹¹⁻¹³), the entire energy level splitting caused by the intermolecular interaction cannot be deduced due to the selection rule governing optical excitations. In principle, the ideal method would be inverse photoelectron spectroscopy (IPES) which detects a photon emitted due to the transition

of an impinging electron from the free-electron state to an unoccupied state in the solid and which is able to probe all the split levels. Yet, conventional IPES ¹⁴ is not precise enough to measure the intermolecular electronic coupling. The typical energy resolution is 0.5 eV, already exceeding the expected intermolecular interaction energy of the order of 100 meV, and the electron bombardment may damage organic samples ¹⁵⁻¹⁶ leading to a poor signal-to-noise ratio if appropriate low electron intensities are applied.

Recently we have developed an experimental technique called low-energy inverse photoelectron spectroscopy (LEIPS) ¹⁷⁻¹⁹. In this technique, the electron energy is lower than the damage threshold of organic molecules ²⁰ to avoid the damage of organic samples. The obtained spectra possess a high signal-to-noise ratio allowing for the analysis of splittings of the LUMO-derived peak. By lowering the electron energy, the emitted photon is in the near-ultraviolet range, which can be analyzed using a high resolution bandpass filter. As a result, an overall resolution of as good as 0.25 eV was attained ¹⁹.

In this study, we experimentally demonstrate the splittings of both HOMO and LUMO-derived levels in a quasi-one-dimensional. At first, we show that tin-phthalocyanine (SnPc) grows in a layer-by-layer fashion on graphite producing quasi-one dimensional columns. Then, the splittings of HOMO and LUMO-derived levels evolving into the one-dimensional band structure are observed using ultraviolet photoelectron spectroscopy (UPS) and LEIPS, respectively, for film thicknesses from 1 to 5 monolayers. Analyzing the data, we evaluate the transfer integrals for both the HOMO and LUMO-derived levels.

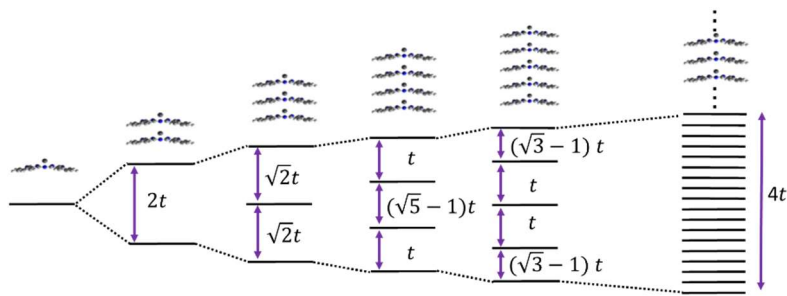


Figure. 1. The energy splittings due to intermolecular orbital interaction. The energy separations are based on the Hückel approximation using the transfer integral t . For increasing chain lengths the bandwidth approaches the value of an infinite chain, being $4t$.

2. Methods

The electronic properties of the SnPc films were measured in Chiba and Okazaki, Japan, using UPS and LEIPS. For this, sublimed-grade SnPc was purchased from NARD Chemicals Ltd and used as received. As a substrate, highly oriented pyrolytic graphite (HOPG, SPI-1 grade) was cleaved in air, and the surface was cleaned by heating in vacuum (10^{-7} Pa) at 673 K over 12 h. The SnPc sample was vacuum-deposited onto the HOPG substrate kept at room temperature and afterwards annealed at 373 K for 1 h, then cooled to room temperature at the natural cooling rate. The average film thickness and deposition rate ($0.05\text{-}0.10$ nm min $^{-1}$) were monitored using a quartz microbalance. Completion of the first monolayer (ML) was determined as disappearance of specific peaks derived from the image potential and from σ^* states of HOPG in LEIPS and metastable atom electron spectroscopy (MAES), respectively. The *in-situ* UPS and LEIPS measurements were conducted in separate vacuum chambers.

For UPS, a HeI light source with a photon energy of 21.218 eV was incident to the sample film kept at room temperature, and the normal emission was detected using a PHOIBOS 100 analyzer (SPECS) with a pass energy of 3 eV and an acceptance angle of $\pm 3^\circ$ in Chiba and a DA30 analyzer (ScientaOmicron) in Okazaki. The total resolution was better than 50 meV and 20 meV, respectively. The LEIPS experiments were carried out in Chiba. Details of the LEIPS apparatus are described elsewhere ²¹. In short, the electron beam with a current of 0.3 μA is incident to the sample along the surface normal, and the emitted photons were analyzed using a bandpass filter (having a center energy of 4.45 eV and a width of 0.17 eV) and a photomultiplier. In order to avoid sample damage due to the electron bombardment, the kinetic energy of the incident electron beam was kept below 5 eV. The energy and angular spread of the electrons were 0.25 eV and 5° , respectively. The overall energy resolution which is determined by the convolution of the electron energy spread and the width of the bandpass filter was about 0.3 eV. Typical measurement time was 2 hours, and no discernible alterations of the spectra due to sample damage were observed.

The crystal structure of the SnPc films was examined in Jena, Germany, using distortion corrected and calibrated low-energy electron diffraction (LEED) ²² as well as differential reflectance spectroscopy (DRS) ²³⁻²⁴. For those experiments, SnPc was provided by Achim Schöll and Christoph Sauer (Würzburg University), purified by gradient sublimation and deposited on single-crystal graphite (obtained from Naturally

Graphite, Michigan Technological University). For DRS, light from a 100 W halogen lamp operated with a stabilized power supply (Müller Elektronik-Optik) is incident to the sample under 20° , measured to the surface normal. The reflected light is then spectrally analyzed by means of a monochromator (Acton Research SpectraPro SP2356) and a charge-coupled device (CCD; Princeton Instruments Spec-10 100BR, liquid-nitrogen-cooled). The measured quantity – the relative change of reflectance during film deposition – is then used to extract the complex dielectric function $\varepsilon(E, d) = \varepsilon'(E, d) - i\varepsilon''(E, d)$ depending on the photon energy E and film thickness d , as described elsewhere²³. After the preparation of SnPc films with varying thicknesses, LEED experiments were performed at room temperature using a dual microchannel plate LEED from OCI Vacuum Microengineering. To achieve quantitative LEED measurements the images were corrected regarding distortions of the raw data, by applying a previously published algorithm,^{22, 25} and subsequently analyzed using the software LEEDLab²⁶.

Throughout the paper, our measurements on SnPc films will be compared to previous ones using the similar, shuttlecock-shaped PbPc molecule. The multitude of data on the structure of PbPc crystals and films helps to understand the structural properties of our samples. Therefore, an energy band calculation of PbPc was performed for the single crystal structures²⁷⁻²⁸ using DMol³ code on the Material Studio program (Accelrys). The Perdew–Burke–Ernzerhof (PBE) functional of the generalized gradient approximation (GGA) with the DNP (double-numeric quality basis set + d-polarization functions for heavy atoms + p-polarization functions for hydrogen atom) basis set was used. The molecular orbitals of single SnPc molecule were calculated using the Becke three-parameter Lee–Yang–Parr exchange–correlation (B3LYP) functional with basis sets of Los Alamos ECP plus MBS for Sn and STO-3G for other atoms in the Gaussian 09 software²⁹.

3. Results and Discussion

3.1. Film Structure

In order to observe the development of energy level splittings as schematically shown in Figure 1, it is necessary to prepare a film consisting of one-dimensional columns containing controlled numbers of molecules. Further, the intermolecular interaction must be large within the columns but negligibly small between the columns.

Planar phthalocyanines often crystallize into one-dimensional columns. However, the

intermolecular orbital overlap is poor, and the transfer integral along the stack is as small as 30 meV³⁰. Therefore, we used a shuttlecock-shape phthalocyanine instead because of the larger intermolecular interaction along the stacking direction. For example, the monoclinic phase of PbPc consists of molecular stacks forming linear columns parallel to the c -axis and exhibits high conductivity along this axis²⁷. In fact, the energy band calculation shows a large sinusoidal dispersion only along the c -axis as shown in Figure 2, characteristic of one-dimensional conductors. The other known polymorph of PbPc is a triclinic phase where the molecules stack with their convex and concave sides alternately pointing up²⁸. In that case, however, the energy band splits in two sub-bands and the dispersion is small (Figure 2b), indicating a strong dimer interaction within the unit cell.

Another requirement for this study is that the substrate should be conductive to avoid the charging of the sample during the electron spectroscopies, while the interaction between the substrate and the molecules should be small. This is almost ideally fulfilled by graphite. If a thin film with a molecular arrangement similar to the monoclinic phase of PbPc were to grow layer-by-layer with the stack axis normal to the substrate, i.e., with the molecular plane parallel to the substrate surface, the evolution of the band structure could be observed using both UPS and LEIPS. Yet, so far monoclinic PbPc films are only reported to grow on polycrystalline Au³¹ and CuI³² surfaces but unfortunately with an edge-on molecular orientation. Further, the molecule-substrate interaction can be expected to be fairly large in those cases. Nevertheless, using the similar shuttlecock phthalocyanine SnPc, we identify a suitable structure in layer-by-layer grown films in which one-dimensional columns align indeed normal to the substrate.

Figure 3a compares the workfunction of PbPc and SnPc films on HOPG as a function of film thickness. The work function decreases until the completion of the first monolayer in both systems and then increases in the case of PbPc, while continuing to decrease with higher layers of SnPc at a slower pace. PbPc and SnPc possess permanent electric dipoles normal to the Pc ring. Thus, the different behavior can be traced back to different molecular orientations. PbPc orients with the concave side down in the first monolayer and then upside down in the second layer to avoid building up a permanent dipole moment in the bilayer⁸. On the other hand, the different behavior of SnPc indicates that the molecules stack in a different manner because the built-up surface dipole of the first ML is retained and slowly increased in thicker layers.

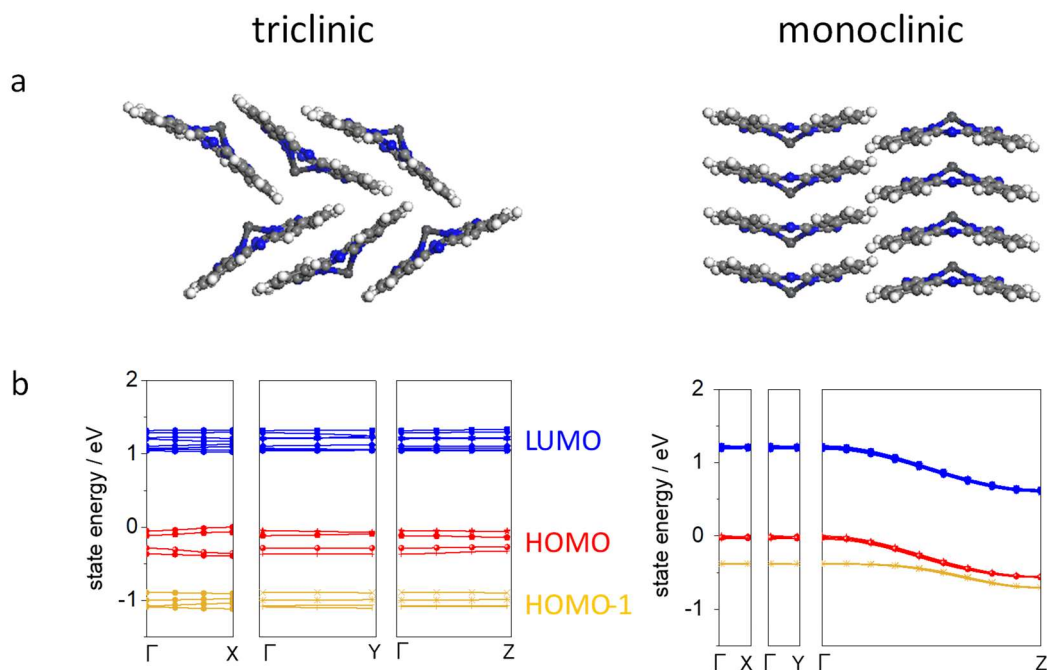


Figure 2. (a) Molecular alignment in the (001) plane of the triclinic²⁸ and the (100) plane of the monoclinic²⁷ crystal phases of PbPc, and (b) the corresponding calculated band structures.

In order to reveal the crystallographic structure of the SnPc film, LEED measurements were performed and the results are shown in Figures 3b and 3c. The two-dimensional lattice parameters are summarized in Table I and compared with those from X-ray diffraction on single crystals^{27-28, 33}. In the first monolayer, the SnPc film adopts the same structure as 1 ML of PbPc on graphite. However, while PbPc was concluded to form a structure on graphite similar to its triclinic polymorph⁸, subsequent layers of SnPc form almost-square unit cells that cannot be found in the triclinic crystal structure of SnPc or PbPc. Furthermore, the surface lattice parameters of a 6 ML SnPc film are similar to the (001) plane of the monoclinic PbPc polymorph²⁷ in the sense that the lattice constants a_1 and a_2 are almost identical to each other and the angle between the \mathbf{a}_1 and \mathbf{a}_2 vectors is nearly 90° . These findings strongly suggest that the SnPc film on graphite is similar to the monoclinic phase of PbPc, and that the SnPc molecules arrange in quasi one-dimensional stacks. However, in contrast to the monoclinic PbPc structure which includes four molecular columns (two with upwards-facing molecules and two with opposite orientation), the SnPc lattice constants allow for only one molecular stack in the unit cell. While this by itself would mean that

all SnPc columns face the same direction, the continued built-up of a surface dipole due to such a uniform arrangement is excluded by the thickness-dependent change of the workfunction, which slows down significantly after the completion of the first ML. The apparent contradiction can be solved by assuming that a random mixture of upwards- and downwards-facing columns coexist. This is consistent with deviations from long-range order in the up/down orientation of molecules reported for monoclinic PbPc crystals ²⁷. Moreover, this effect does not render our conclusions about the electronic structure invalid, as we will discuss later. Note also that our structure stands out because even though there are many reports of SnPc film structures, such as for SnPc on HOPG(0001) ³⁴, Ag(111) ³⁵⁻³⁶ and 1 ML PTCDA/Ag(111) ³⁷, a monoclinic-like unit cell has not been reported so far for SnPc.

In order to further validate the structure, optical absorption spectroscopy shall be briefly discussed in the following, since it is sensitive to the molecular packing and is an established method to identify different polymorphs of phthalocyanines ^{32, 37-38}. In the case of PbPc, the Q-band of monomers is observed around 1.68 eV ³⁹. The absorption maximum red-shifts only slightly to 1.65 eV in monoclinic PbPc, while in the triclinic phase the band splits strongly and the main peak is observed at 1.35 eV representing a large red-shift of 0.4 eV ⁴⁰. Likewise, a triclinic-like SnPc thin film ³⁷ has been reported to feature the strongest absorption around 1.37 eV.

We measured the optical absorption of the Q-band region of SnPc thin films on graphite as a function of film thickness using *in-situ* DRS as shown in Figure 3d. In the submonolayer range, the SnPc spectra are dominated by a main peak at 1.7 eV assignable to the monomeric SnPc Q-band and a high-energy shoulder, as can be expected of the monomer-like absorption of flatly adsorbed, hardly interacting molecules. Upon completion of the 1st ML the peak shifts by 0.1 eV to 1.6 eV, indicating a stronger interaction of optical transition dipoles between the stacked layers. However, the spectral line shape is strongly different from triclinic SnPc ³⁷ and resembles those of monoclinic PbPc, which corroborates a similar molecular arrangement as already deduced from LEED measurements.

According to the LEED and DRS results, together with the thickness dependence of the workfunction, we conclude that SnPc on HOPG grows in quasi one-dimensional columns similar to the monoclinic phase of PbPc single crystals.

It should be noted that the polymorph formed is very sensitive to the growth conditions of the film and the substrate surface. In fact, we sometimes observed films partly featuring broad LEED spots and DRS signatures of a triclinic-like structure. In order to fabricate the quasi one-dimensional columns consisting of either concave or convex stacking of SnPc molecules, we need the monoclinic film since the triclinic film contains alternative convex and concave molecular packings. As deduced from LEED and DRS results, the as-deposited films consist predominantly of the monoclinic phase while the films annealed beyond 400 K are in the triclinic phase (Figure 3d). Films deposited on substrates kept at higher than room temperature also show the triclinic phase. Thus the monoclinic phase of SnPc is assumed to be metastable. Fortunately, the line shape of UPS correlates well with the polymorphs (Figure S4 in the Supporting Information) which facilitates a clear distinction. Therefore, in each electron spectroscopy measurement, we confirmed the polymorph of the obtained film from the line shapes of UPS.

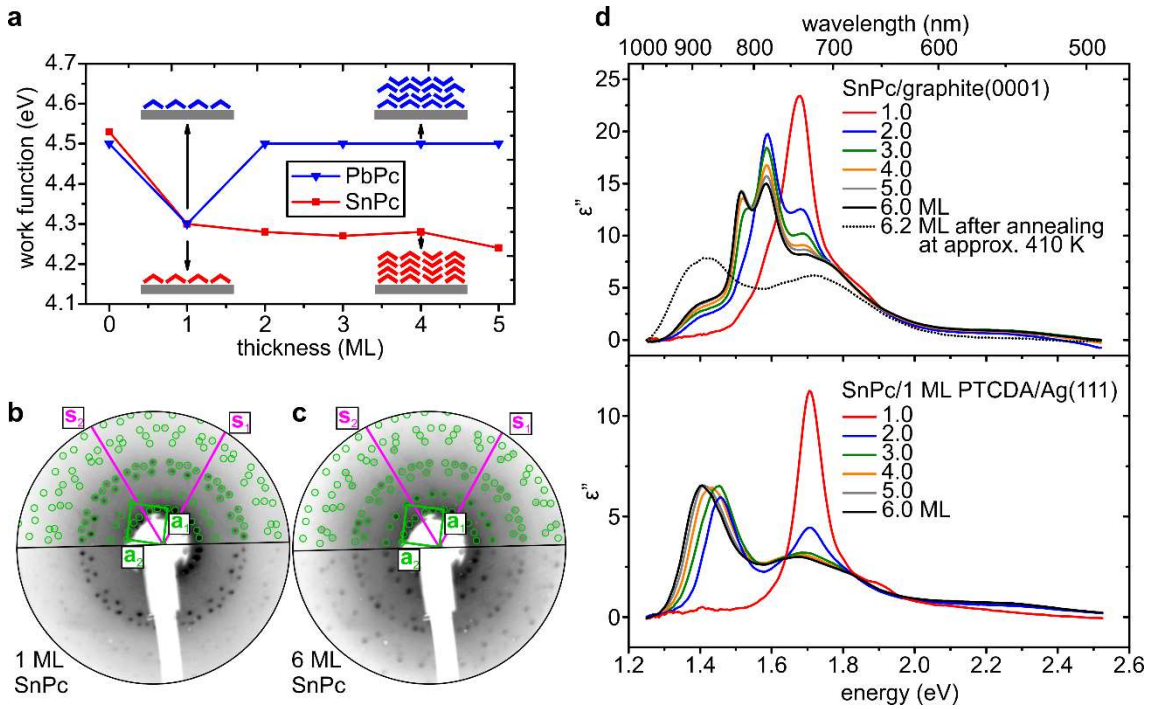


Figure 3. (a) Workfunctions of SnPc and PbPc films as a function of the number of layers. (b),(c) LEED patterns of 1 ML and 6 ML SnPc on graphite, respectively (contrast logarithmic, inverted). The direction of the substrate unit cell vectors is indicated in magenta, diffraction orders due to SnPc are marked in green. (d) Thickness-dependent imaginary part ϵ'' of the dielectric function of SnPc on graphite during deposition and

after annealing at 410 K, respectively (top panel), compared to triclinic SnPc on 1 ML PTCDA on Ag(111) (bottom panel ³⁷).

TABLE. I. Lattice constants of PbPc and SnPc films on graphite and in single crystals.

	a_1 (Å)	a_2 (Å)	$\angle a_1, a_2$ (deg)
PbPc 1 ML ⁴¹	13.8(2)	13.9(2)	92.1(1)
SnPc 1 ML	13.8(3)	13.9(3)	91.7(1)
SnPc 2 ML	13.7(1)	13.7(1)	90.4(1)
SnPc 6 ML	13.64(13)	13.65(13)	90.1(1)
(001) plane of monoclinic PbPc ^{a)}	25.48 ^{d)}	25.48 ^{d)}	90
(010) plane of triclinic PbPc ^{b)}	13.12	12.89	96.20
(10-1) plane of triclinic SnPc ^{c)}	12.62	14.22	104.64

a) Ref. 27, b) Ref. 28, c) Ref. 33, d) The unit cell contains 2 upwards facing and 2 downwards facing molecular columns.

3.2. Electronic Structure

After clarifying the structural properties of the SnPc/graphite films, UPS and LEIPS were applied to examine the occupied and unoccupied energy levels, respectively. Figure 4 shows the spectra of films with thicknesses between 1 and 5 ML and annealed at 373 K. The respective data sets for as-deposited samples are shown in Figure S3 in the Supporting Information. Based on the calculated energy levels of a single SnPc molecule belonging to the C_{4v} point group, the peaks observed at -2.4 eV, -1.3 eV and 1.1 eV are assigned to the HOMO-1 (a_1), HOMO (a_2) and LUMO (e)-derived levels, respectively. As the film thickness increases, the width of each peak also increases.

First, we analyze the difference in the spectra of 1 ML and 2 ML in detail. As we demonstrated previously in the case of PbPc bilayers on HOPG ⁸, we could reproduce each peak of the 2 ML film as the sum of a corresponding peak from the 1 ML film and a slightly shifted copy of it, to mimic an assumed orbital splitting due to intermolecular interaction within molecular dimers. As shown in Figure 4, also the 2 ML spectra of SnPc show excellent agreement with the superposition of two 1 ML spectra with energy separations of 203 (190) and 256 (243) meV for the annealed (as-deposited) HOMO and

LUMO, respectively, while the separation is less than 10 meV for the HOMO-1. Assuming the energy splitting is twice the transfer integral t according to the Hückel approximation, we calculated the transfer integrals as $t_{\text{HOMO-1}} = 5$ meV, $t_{\text{HOMO}} = 102$ (95) meV, and $t_{\text{LUMO}} = 128$ (122) meV. Based on multiple data taken under different experimental conditions, we evaluate the transfer integrals as $t_{\text{HOMO-1}} < 5$ meV, $t_{\text{HOMO}} = 100$ meV and $t_{\text{LUMO}} = 128$ meV, respectively, with uncertainties of 10 meV (see Tables S1 and S2 and associated text in the Supporting Information for the evaluation of the values). Some larger deviation between experimental and fitted spectra, especially noticeable for the larger film thicknesses of the as-deposited films, is most probably caused by the higher degree of disorder. This means in turn that the broadening of the 2 ML spectrum of the annealed film in Figure 4 represents a peak splitting predominantly caused by the intermolecular orbital interaction and not by inhomogeneous broadening which is negligible here (Figure S3 in the Supporting Information).

Now that the transfer integrals along the stacking direction in a dimer are obtained, we will discuss the thickness-dependent spectral line shape for film thicknesses of 3 ML and beyond. As mentioned above, the separations between the energy levels in chains of different numbers of molecules can be calculated as in Figure 1 within the framework of the Hückel approximation. The transfer integral t has been obtained for each orbital from the spectra of the bilayer as outlined above. Based on these values, we simulate the spectral line shape as a sum of spectral features of the 1 ML film in Figure 4a. The agreement with the experimental data is excellent in all cases. We emphasize that the only free parameters are the normalization factor of the peak intensity and the center energy of the peak. The relative intensity of the components is kept fixed. The energy separations of the peaks are determined by the Hückel method (Figure 1) using the experimentally determined transfer integrals from the dimers. This finding supports the conclusion that SnPc grows indeed predominantly layer-by-layer in quasi-one-dimensional stacks on HOPG, and the broadening of the peaks is really caused by intermolecular orbital interaction, as the good agreement over the whole range of film thickness cannot be accidental.

Yet, as the film thickness increases (particularly to 4 and 5 ML), certain differences between the modelled and experimental spectra become discernible. SnPc molecules often show island growth in multilayers, i.e., Stranski-Krastanov growth⁴²⁻⁴⁴. Therefore, a commencing inhomogeneity in the film thickness may give rise to the slight

disagreement between the simulated and experimental results in multilayers. We also assessed the limitation of the simple Hückel approximation, i.e., the neglect of the overlap integral and the inclusion of only the nearest-neighbor transfer integrals. The extended Hückel method including the overlap integral gives essentially the same energy separations. Since the wavefunction decays exponentially with the distance, the transfer integral between the next-nearest neighbor molecules should already be negligible, as exemplified by the DFT calculation of pentacene ⁷.

Finally, we want to discuss the small transfer integral in the HOMO-1-derived level, which may be surprising at the first glance. Figure 4b shows the molecular SnPc orbitals of the HOMO-1, HOMO, and LUMO as calculated by DFT. The HOMO and LUMO are π -orbitals being delocalized over the phthalocyanine ligand, while the HOMO-1 is localized on the metal atom and extends only to the concave side. Consequently, the intermolecular overlap should be much smaller for the HOMO-1 than for both the HOMO and the LUMO in a one-dimensional column. Such differences in the shape of molecular orbitals should also affect the angular dependence of UPS and LEIPS intensities. The HOMO and LUMO intensities increase with the number of layers while the HOMO-1 bands intensity decreases from 1 ML to 2 ML. This anomaly in the intensities is likely due to the difference in the molecular orientation in 1 ML and the multilayer as discussed above.

Further, the observed transfer integrals are larger for the LUMO than for the HOMO indicating the larger overlap between the LUMOs of nearest-neighbor molecules along the stack compared to the HOMO. Actually, the wavefunctions of the HOMO and LUMO appear rather similar in terms of the number of nodes in Figure 4b. The calculated bandwidths in Figure 2 are also slightly larger for the LUMO (0.59 eV) than for the HOMO (0.54 eV). This suggests that the spatial extension of unoccupied orbitals is larger due to the smaller shielding of the positive charges of the atomic cores by the valence electrons. Note that the difference in the instrumental resolution does not affect the transfer integrals as discussed in Section 5 of the Supporting Information.

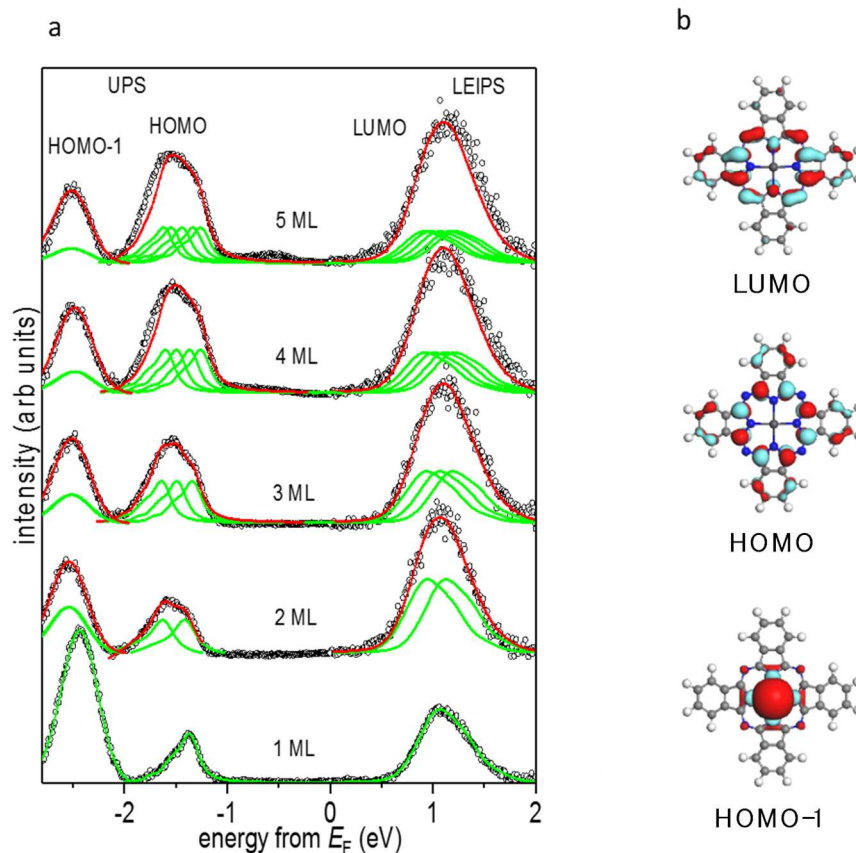


Figure 4a. Electronic structure of SnPc films with reference to the Fermi level E_F . (a) The combined UPS and LEIPS spectra of SnPc/HOPG, with the thickness ranging between 1 and 5 ML. The experimental data (open circles) are reproduced with the sum (red lines) of several spectral line shapes of the 1 ML peak (green lines) based on the energy levels calculated by our Hückel model (see Figure 1 and text). (b) Calculated molecular orbitals of SnPc.

4. Conclusion

We successfully prepared layers consisting of quasi-one-dimensional stacks of SnPc on graphitic surfaces with a well-defined number of layers in the range between 1 and 5 ML. We examined the HOMO-1, HOMO and LUMO-derived energy levels using UPS and LEIPS. The observed evolution of the peak shape and width is interpreted as an orbital splitting caused by intermolecular orbital interaction. The transfer integrals for the HOMO-1, HOMO and LUMO are determined to be < 15 meV, $t_{\text{HOMO}} = (100 \pm 10)$ meV and $t_{\text{LUMO}} = (128 \pm 10)$ meV, respectively, in the framework of the Hückel approximation which was applied here. The differences in the magnitudes of the transfer integrals can be understood by considering the spatial extension of molecular orbitals.

Corresponding Author

Hiroyuki Yoshida Email: hyoshida@chiba-u.jp

Satoshi Kera Email: kera@ims.ac.jp

Torsten Fritz Email: torsten.fritz@uni-jena.de

Acknowledgements

We thank Mr. Ryo Shiraishi of IMS for his technical assistance in the PbPc band calculation. Computation time was provided by the SuperComputer System, Institute for Chemical Research, Kyoto University. This research was supported by JSPS KAKENHI (Grant Numbers 26288007 and 26248062), and was partially founded by the DFG (Grant Numbers FO 770/2-1 and FR 875/16-1).

Supporting Information

DRS raw data; raw UPS and LEIPS spectra and background removal; UPS and LEIPS spectra of as-deposited SnPc/HOPG; SnPc polymorphs and line shapes of UPS; uncertainties in the transfer integrals; effect of the energy resolution of the apparatus on the transfer integrals

References

1. Coropceanu, V.; Cornil, J.; da Silva, D. A.; Olivier, Y.; Silbey, R.; Bredas, J. L., Charge Transport in Organic Semiconductors. *Chem. Rev.* **2007**, *107*, 926-952.
2. Silinsh, E. A., *Organic Molecular Crystals: Their Electronic States*. Springer Science & Business Media: 2012; Vol. 16.
3. Ueno, N.; Kera, S., Electron Spectroscopy of Functional Organic Thin Films: Deep Insights into Valence Electronic Structure in Relation to Charge Transport Property. *Prog. Surf. Sci.* **2008**, *83*, 490-557.
4. Yamane, H.; Kosugi, N., Substituent-Induced Intermolecular Interaction in Organic Crystals Revealed by Precise Band-Dispersion Measurements. *Phys. Rev. Lett.* **2013**, *111*, 086602.
5. Hoffmann, R., *Solids and Surfaces: A Chemist's View of Bonding in Extended Structures*. VCH Publishers: New York, 1988.
6. Hoffmann, M.; Schmidt, K.; Fritz, T.; Hasche, T.; Agranovich, V. M.; Leo, K., The Lowest Energy Frenkel and Charge-Transfer Excitons in Quasi-One-Dimensional Structures: Application to MePTCDI and PTCDA Crystals. *Chem. Phys.* **2000**, *258*, 73-96.
7. Yoshida, H.; Sato, N., Crystallographic and Electronic Structures of Three Different Polymorphs of Pentacene. *Phys. Rev. B* **2008**, *77*, 235205.
8. Kera, S.; Fukagawa, H.; Kataoka, T.; Hosoumi, S.; Yamane, H.; Ueno, N., Spectroscopic Evidence of Strong π - π Interorbital Interaction in a Lead-Phthalocyanine Bilayer Film Attributed to the Dimer Nanostructure. *Phys. Rev. B* **2007**, *75*, 121305.
9. Wang, C. L.; Dong, H. L.; Hu, W. P.; Liu, Y. Q.; Zhu, D. B., Semiconducting π -Conjugated Systems in Field-Effect Transistors: A Material Odyssey of Organic Electronics. *Chem. Rev.* **2012**, *112*, 2208-2267.
10. Anthony, J. E.; Facchetti, A.; Heeney, M.; Marder, S. R.; Zhan, X. W., N-Type Organic Semiconductors in Organic Electronics. *Adv. Mater.* **2010**, *22*, 3876-3892.
11. Bredas, J. L.; Cornil, J.; Heeger, A. J., The Exciton Binding Energy in Luminescent Conjugated Polymers. *Advanced Materials* **1996**, *8*, 447-452.
12. Knupfer, M.; Fink, J., Frenkel and Charge-Transfer Excitons in C₆₀. *Phys. Rev. B* **1999**, *60*, 10731-10734.
13. Djurovich, P. I.; Mayo, E. I.; Forrest, S. R.; Thompson, M. E., Measurement of the Lowest Unoccupied Molecular Orbital Energies of Molecular Organic Semiconductors. *Org. Electron.* **2009**, *10*, 515-520.
14. Dose, V., VUV Isochromat Spectroscopy. *Appl. Phys.* **1977**, *14*, 117-118.
15. Tsutsumi, K.; Yoshida, H.; Sato, N., Unoccupied Electronic States in a

- Hexatriacontane Thin Film Studied by Inverse Photoemission Spectroscopy. *Chem. Phys. Lett.* **2002**, 361, 367-373.
16. Li, Z.; Sun, S. Q.; Li, X.; Schlaf, R., The Impact of Inverse Photoemission Spectroscopy Measurements on Regioregular Poly(3-Hexylthiophene) Films. *Appl. Phys. Lett.* **2014**, 104, 021606.
 17. Yoshida, H., Near-Ultraviolet Inverse Photoemission Spectroscopy Using Ultra-Low Energy Electrons. *Chem. Phys. Lett.* **2012**, 539-540, 180-185.
 18. Yoshida, H., Measuring the Electron Affinity of Organic Solids: An Indispensable New Tool for Organic Electronics. *Anal. Bioanal. Chem.* **2014**, 406, 2231-2237.
 19. Yoshida, H., Principle and Application of Low Energy Inverse Photoemission Spectroscopy: A New Method for Measuring Unoccupied States of Organic Semiconductors. *J. Elec. Spec. Relat. Phenom.* **2015**, 204, 116-124.
 20. Boudaiffa, B.; Cloutier, P.; Hunting, D.; Huels, M. A.; Sanche, L., Resonant Formation of DNA Strand Breaks by Low-energy (3 to 20 eV) Electrons. *Science* **2000**, 287, 1658-1660.
 21. Yoshida, H., Note: Low Energy Inverse Photoemission Spectroscopy Apparatus. *Rev. Sci. Instrum.* **2014**, 85, 016101.
 22. Sojka, F.; Meissner, M.; Zwick, C.; Forker, R.; Fritz, T., Determination and Correction of Distortions And Systematic Errors in Low-Energy Electron Diffraction. *Rev. Sci. Instrum.* **2013**, 84, 015111.
 23. Forker, R.; Gruenewald, M.; Fritz, T., Optical Differential Reflectance Spectroscopy on Thin Molecular Films. *Annu. Rep. C* **2012**, 108, 34-68.
 24. Forker, R.; Fritz, T., Optical Differential Reflectance Spectroscopy of Ultrathin Epitaxial Organic Films. *Phys. Chem. Chem. Phys.* **2009**, 11, 2142-2155.
 25. Sojka, F.; Meissner, M.; Zwick, C.; Forker, R.; Vyshnepolsky, M.; Klein, C.; Horn-von Hoegen, M.; Fritz, T., To Tilt or Not to Tilt: Correction of The Distortion Caused by Inclined Sample Surfaces in Low-Energy Electron Diffraction. *Ultramic.* **2013**, 133, 35-40.
 26. The software 'LEEDLab' version 1.64 is commercially available from ScientaOmicron at <http://www.scientaomicron.com/en/products/350/1155>.
 27. Ukei, K., Lead Phthalocyanine. *Acta Cryst. B* **1973**, 29, 2290-2292.
 28. Iyechika, Y.; Yakushi, K.; Ikemoto, I.; Kuroda, H., Structure of Lead Phthalocyanine (Triclinic Form). *Acta Cryst. B* **1982**, 38, 766-770.
 29. Frisch, M.; Trucks, G.; Schlegel, H.; Scuseria, G.; Robb, M.; Cheeseman, J.; Scalmani, G.; Barone, V.; Mennucci, B.; Petersson, G. et al, Gaussian 09, Rev. A. 02.

Gaussian Inc., Wallingford, CT **2009**.

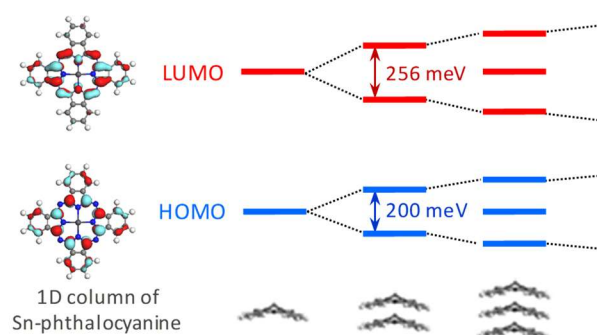
30. Yamane, H.; Kosugi, N., Substituent-Induced Intermolecular Interaction in Organic Crystals Revealed by Precise Band-Dispersion Measurements. *Phys. Rev. Lett.* **2013**, *111*, 086602.
31. Miyamoto, A.; Nichogi, K.; Taomoto, A.; Nambu, T.; Murakami, M., Structural control of Evaporated Lead-Phthalocyanine Films. *Thin Solid Films* **1995**, *256*, 64-67.
32. Kim, T. M.; Kim, H. J.; Shim, H. S.; Choi, M. S.; Kim, J. W.; Kim, J. J., The Epitaxial Growth of Lead Phthalocyanine on Copper Halogen Compounds as the Origin of Templating Effects. *J. Mater. Chem. A* **2014**, *2*, 8730-8735.
33. Friedel, M.; Hoskins, B.; Martin, R.; Mason, S., A New Metal (II) Phthalocyanine Structure: X-ray and Mössbauer Studies of the Triclinic Tin (II) Phthalocyanine. *J. Chem. Soc. D* **1970**, 400-401.
34. Walzer, K.; Hietschold, M., STM and STS Investigation of Ultrathin Tin Phthalocyanine Layers Adsorbed on HOPG(0001) and Au(111). *Surf. Sci.* **2001**, *471*, 1-10.
35. Lackinger, M.; Hietschold, M., Determining adsorption geometry of individual Tin-Phthalocyanine Molecules on Ag(111) - a STM Study at Submonolayer Coverage. *Surf. Sci.* **2002**, *520*, L619-L624.
36. Schwarz, F.; Wang, Y. F.; Hofer, W. A.; Berndt, R.; Runge, E.; Kroger, J., Electronic and Vibrational States of Single Tin-Phthalocyanine Molecules in Double Layers on Ag(111). *J. Phys. Chem. C* **2015**, *119*, 15716-15722.
37. Gruenewald, M.; Peuker, J.; Meissner, M.; Sojka, F.; Forker, R.; Fritz, T., Impact of a Molecular Wetting Layer on the Structural and Optical Properties of Tin (II)-Phthalocyanine Multilayers on Ag (111). *Phys. Rev. B* **2016**, *93*, 115418.
38. Vasseur, K.; Broch, K.; Ayzner, A. L.; Rand, B. P.; Cheyins, D.; Frank, C.; Schreiber, F.; Toney, M. F.; Froyen, L.; Heremans, P., Controlling the Texture and Crystallinity of Evaporated Lead Phthalocyanine Thin Films for Near-Infrared Sensitive Solar Cells. *ACS Appl. Mater. Interfaces* **2013**, *5*, 8505-8515.
39. Kumar, T. M.; Achar, B., Synthesis and Characterization of Lead Phthalocyanine and its Derivatives. *J. Organomet. Chem.* **2006**, *691*, 331-336.
40. Miyamoto, A.; Nichogi, K.; Taomoto, A.; Nambu, T.; Murakami, M., Structural Control of Evaporated Lead-Phthalocyanine Films. *Thin Solid Films* **1995**, *256*, 64-67.
41. Kawakita, N.; Yamada, T.; Meissner, M.; Forker, R.; Fritz, T.; Munakata, T., Metastable Phase of Lead Phthalocyanine Films on Graphite: Correlation between Geometrical and Electronic Structures. *Phys. Rev. B* **2017**, *95*, 045419.
42. Wang, S.; Dong, X.; Lee, C.; Lee, S., Orderly Growth of Copper Phthalocyanine

on Highly Oriented Pyrolytic Graphite (HOPG) at High Substrate Temperatures. *J. Phys. Chem. B* **2004**, 108, 1529-1532.

43. Vearey-Roberts, A.; Steiner, H.; Evans, S.; Cerrillo, I.; Mendez, J.; Cabailh, G.; O'Brien, S.; Wells, J.; McGovern, I.; Evans, D., Growth and Morphology of SnPc Films on the S-GaAs (001) Surface: A Combined XPS, AFM and NEXAFS Study. *Appl. Surf. Sci.* **2004**, 234, 131-137.

44. Jung Kim, H.; Shim, H.-S.; Whan Kim, J.; Hwi Lee, H.; Kim, J.-J., CuI Interlayers in Lead Phthalocyanine Thin Films Enhance Near-Infrared Light Absorption. *Appl. Phys. Lett.* **2012**, 100, 134.

Graphics for TOC



Quantum chemistry shows how an energy level splits into two levels in molecular dimers, into three levels in trimers and evolves into an energy band in infinite systems. Fabricating one-dimensional stacks of tin-phthalocyanine with a controlled number of molecules, we demonstrate splittings of both HOMO and LUMO using ultraviolet photoelectron and low-energy inverse photoelectron spectroscopies. The results are analyzed based on the Hückel method.

Supplemental Information

The Evolution of Intermolecular Energy Bands of Occupied and Unoccupied Molecular States in Organic Thin Films

Yuki Kashimoto¹, Keiichirou Yonezawa², Matthias Meissner^{2,3}, Marco Gruenewald³,
Takahiro Ueba², Satoshi Kera^{1,2*}, Roman Forker³,
Torsten Fritz^{3*}, Hiroyuki Yoshida^{1,4*}

¹*Graduate School of Engineering, Chiba University, 1-33, Yayoi-cho, Inage-ku, Chiba
263-8522, Japan*

²*Institute for Molecular Science, Myodaiji, Okazaki, 444-8585, Japan*

³*Institut für Festkörperphysik, Friedrich-Schiller-Universität Jena, Helmholtzweg 5,
07743 Jena, Germany*

⁴*Molecular Chirality Research Center, Chiba University, 1-33, Yayoi-cho, Inage-ku,
Chiba 263-8522, Japan*

Contents

1. DRS raw data
2. Raw UPS and LEIPS spectra and the background removal
3. UPS and LEIPS spectra of as-deposited SnPc/HOPG
4. SnPc polymorphs and line shapes of UPS
5. Uncertainties in the transfer integrals
6. Effect of the energy resolution of the apparatus on the transfer integrals

1. Raw DRS data

The imaginary part ε'' of the dielectric function $\hat{\varepsilon} = \varepsilon' - i\varepsilon''$ of SnPc/graphite(0001) is shown for different film thicknesses in the main text. For the sake of completeness, the raw data that was used for the determination of $\hat{\varepsilon}$ is shown in Figure S1.

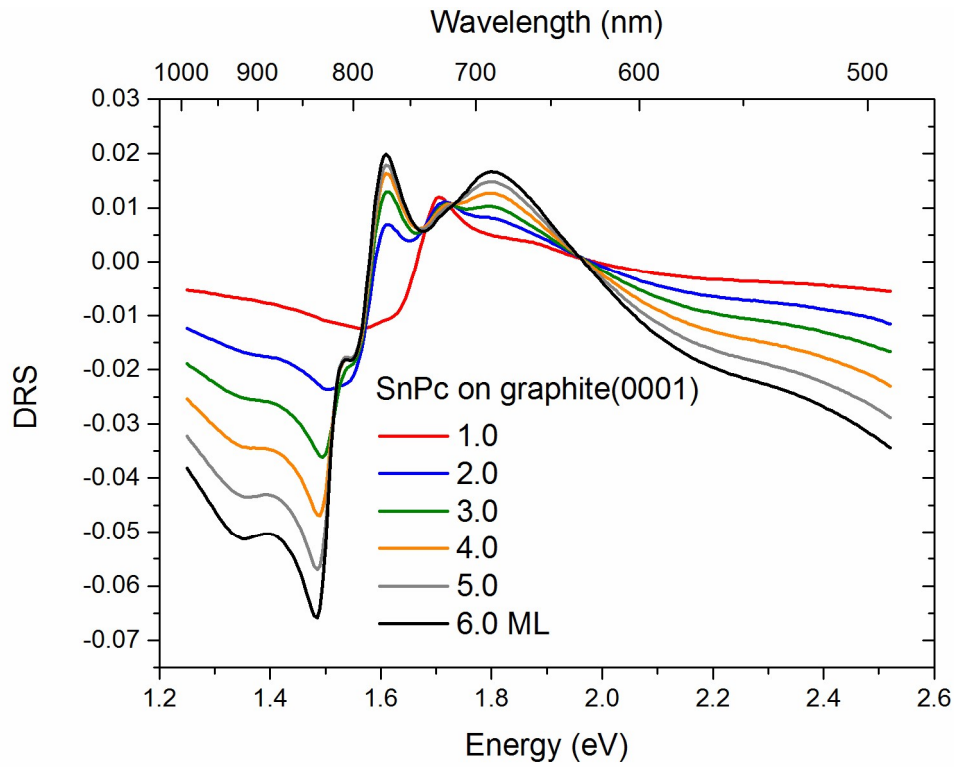


Figure S1. Raw DRS data for SnPc/graphite(0001) measured *in situ* during film deposition.

2. Raw UPS and LEIPS spectra and background removal

Figure S2 shows the raw UPS and LEIPS spectra of the SnPc films on HOPG. The background signal of each peak was simply approximated by a linear background and subsequently subtracted. The background-subtracted spectra of annealed and as-deposited films are shown in Figures 4b and S3, respectively.

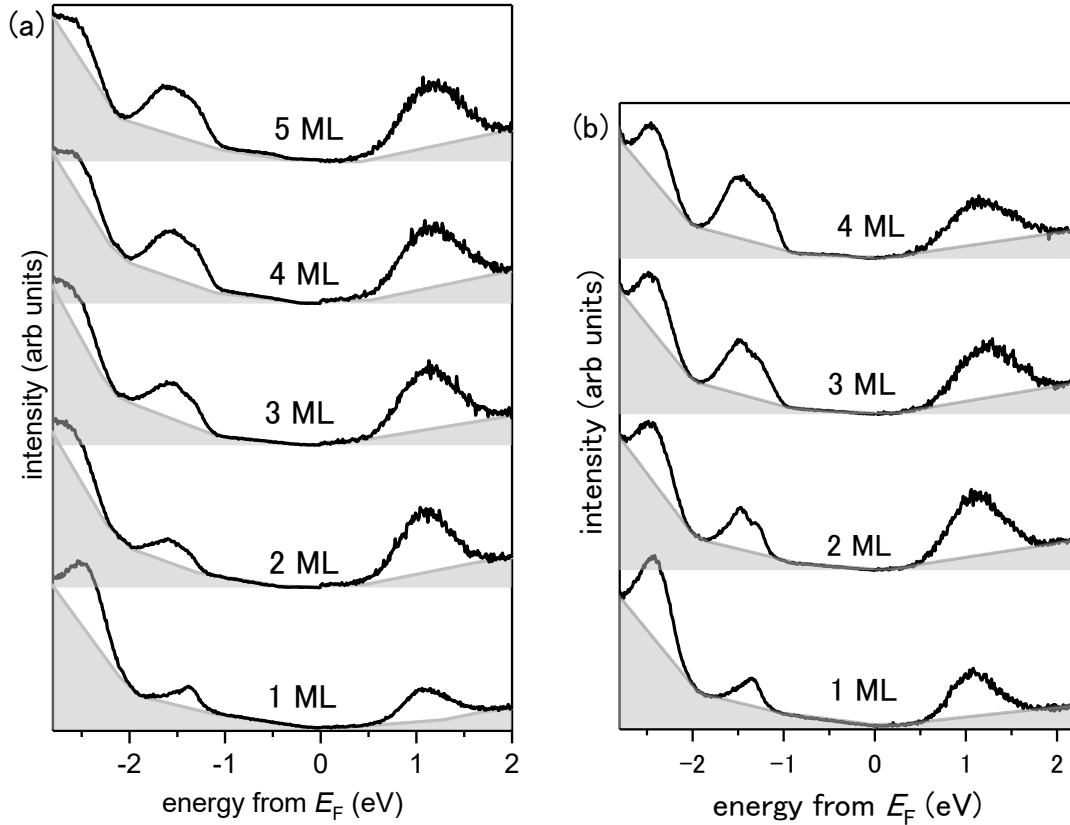


Figure S2. Raw UPS and LEIPS spectra (a) for the annealed and (b) as-deposited SnPc/HOPG. The black lines show the raw data, and the grey shaded areas are the backgrounds.

3. UPS and LEIPS spectra of as-deposited SnPc/HOPG

We analyzed the spectra of as-deposited films applying the same procedure as we employed in Figure 4a. The obtained transfer integrals are summarized in Tables S1 and S2 for HOMO and LUMO, respectively.

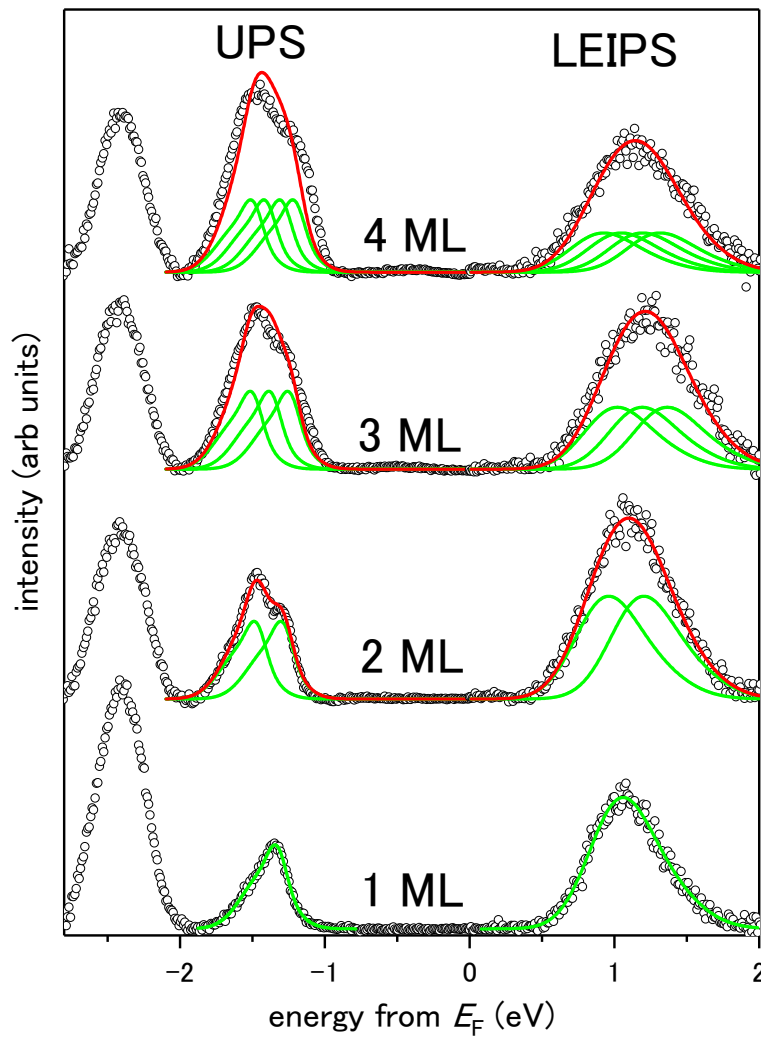


Figure S3. Combined UPS and LEIPS spectra of as-deposited SnPc films. The experimental data (open circles) are reproduced with the sum (red lines) of several spectral line shapes of the 1 ML peak (green lines).

4. Polymorphs and line shapes of UPS

In order to discuss the relation between the SnPc polymorphs and the spectral line shapes of UPS we prepared another set of as-deposited and annealed (at 350 K for about 30 min) films of 3 to 4 ML SnPc on graphite. The occurring polymorphs are examined by LEED as shown in Figure S4. The as-deposited film shows the diffraction spots of the monoclinic phase while the annealed film contains another unknown phase.

For the same sample films we performed high-resolution UPS on the Scienta-Omicron DA30 in Okazaki. The peak widths and line shapes are different between the as-deposited and annealed films, meaning that the spectral line shape of UPS is sensitive to the polymorphs of the film. The full width at half maximum (FWHM) of the HOMO peak is 490 meV which is 100 meV smaller than that of the as-deposited film (590 meV). Since the LEED results suggest that the annealed film contains the monoclinic phase plus another component, we subtracted the spectrum of the as-deposited film from that of the annealed one to obtain the spectrum of the new component. The difference spectrum shows a doublet peak with a separation of about 300 meV suggesting the existence of intermolecular electronic coupling only within molecular dimers. In fact, the doublet peak is similar to the 2 ML spectrum of the triclinic phase (not shown). The film may contain dimers of SnPc molecules with the convex-concave stacking described in the main paper; the situation may be similar to the bandstructure of the triclinic phase of PbPc showing the splitting of HOMO and LUMO bands in Figure 2.

Based on the above results, we can distinguish the polymorphs of the SnPc films from the line shape and peak widths. The UPS spectra shown in Figures 4a and S3 are similar to that of the as-deposited film from Figure S4c (monoclinic) but different from that of the annealed film in Figure S4d (mixture). These findings confirm that the SnPc films of Figures 4 and S3 consist of the monoclinic phase.

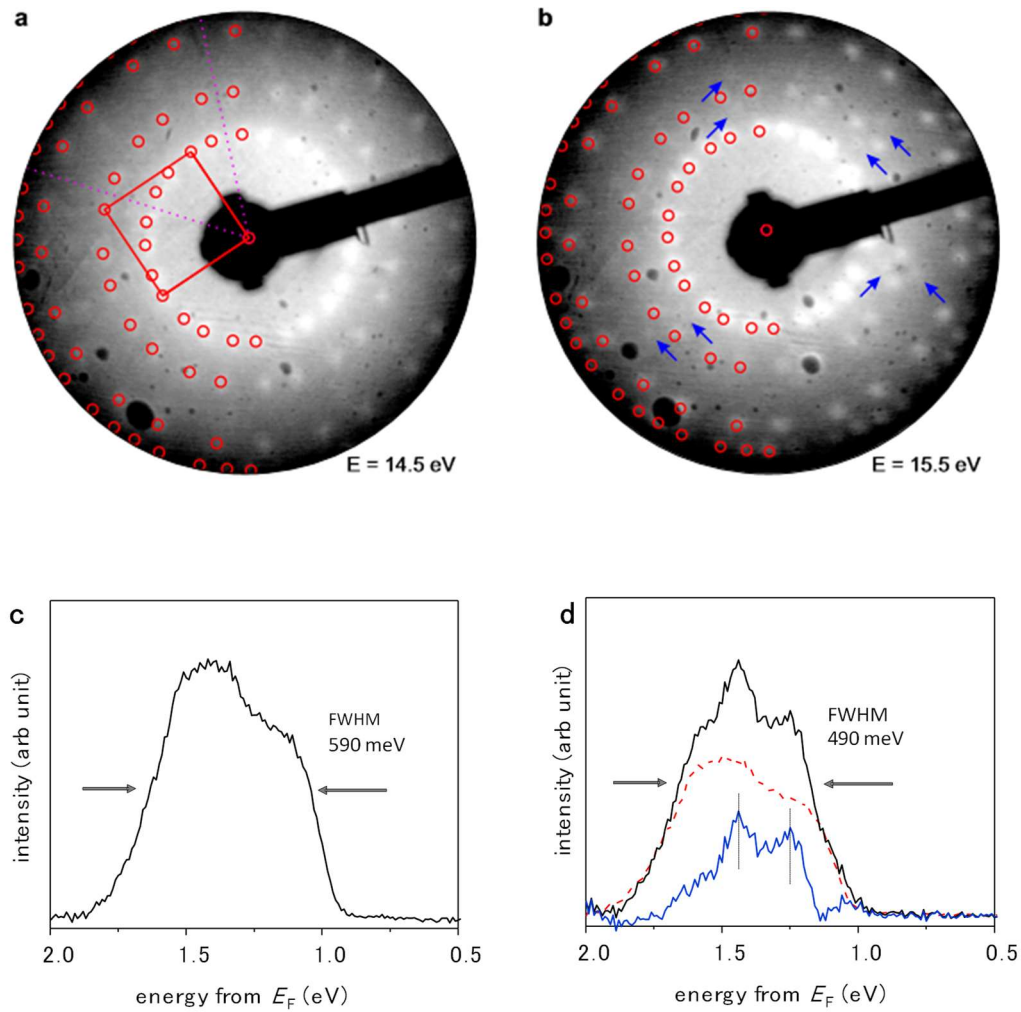


Figure S4. Comparison between LEED images (logarithmic contrast, corrected for radial distortion¹) of a 3 to 4 ML SnPc film acquired at room temperature on single-crystalline graphite (SCG) in the as-deposited state (a) and after annealing at 350 K for ~ 30 min (b). Red circles in the LEED images mark spots of the monoclinic SnPc structure, blue arrows mark spots corresponding to a different yet unknown structure. The UPS spectra observed for the same as-deposited (c) and annealed (d) samples are shown by black solid lines. In panel (d), the difference spectrum (blue solid line) between the observed spectra for the annealed film (black solid line) and the as-deposited film taken from panel c (red dashed line) may originate from the new structure appearing by the annealing treatment.

5. Uncertainties in the transfer integrals

Transfer integrals were obtained by fitting the spectra with the spectral line shapes of the 1-ML peak to the spectra of 2-ML films. There are several origins of the uncertainties in the transfer integrals. The only free parameters in the fitting procedure were the positions of the peaks and the intensity of the peak with fixed relative intensities. The statistically estimated error was less than 5 meV.

The nominally 2 ML film may not grow perfectly in a layer-by-layer mode and may contain monolayer regions. We analyzed the spectrum of the 2 ML film using the doublet due to the intermolecular electronic coupling and a fraction of the spectral contribution from the monolayer. It turned out that adding the monomer component to the doublet increases the transfer integral. Figure S5 shows the analyzed data with the doublet and different portions of the 1 ML component for the UPS spectra of the annealed sample. As shown in Tables S1 and S2, adding 20% of the 1 ML component increases each transfer integral by about 8 meV. As mentioned in the main text, we carefully determined the thickness of 1 ML from the disappearance of a specific peak of graphite. The uncertainty in the thickness of 2 ML is at most 20%.

It is also found that the transfer integral varies and seems to depend on the quality of the film. For example, the transfer integral of the HOMO is in the range between 91.5 meV and 101.5 meV at room temperature. The largest value was obtained for the annealed sample.

From the above considerations, we estimate the uncertainty as 10 meV.

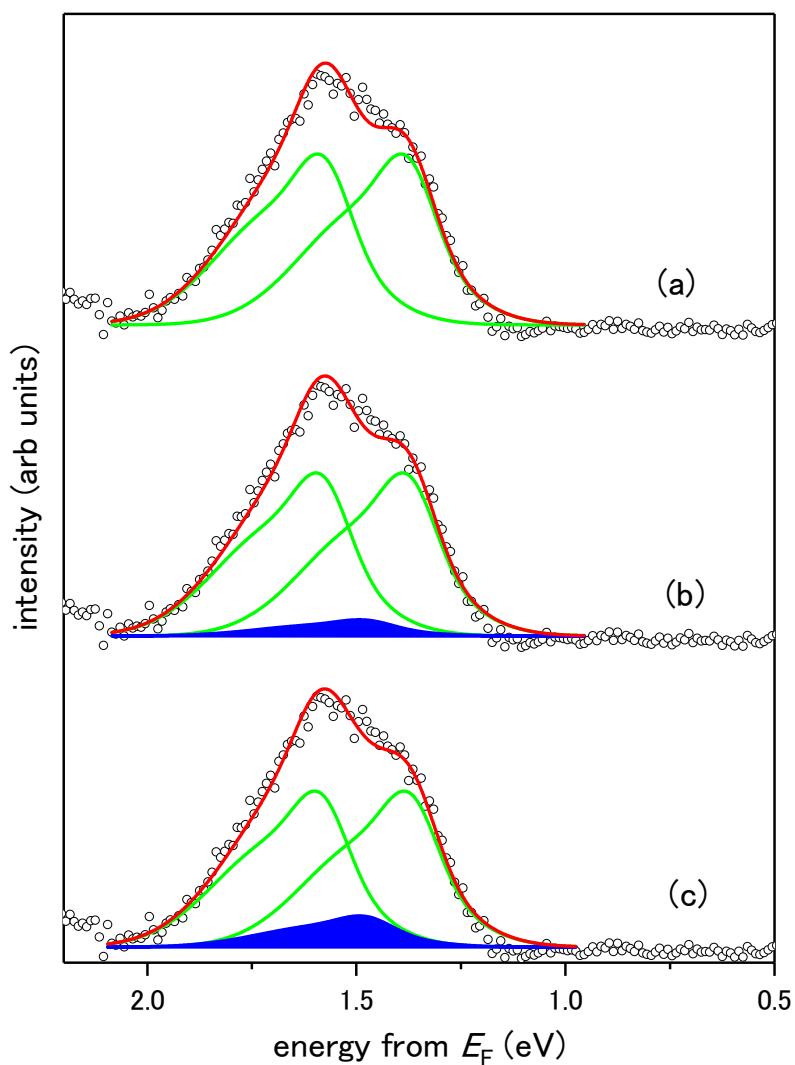


Figure S5. Analysis of the 2 ML spectra including the non-shifted spectral component from the 1 ML region. (a) 2 ML spectrum fitted by two 1 ML line shapes (green lines) without the 1 ML component, (b) the doublet spectrum with 10% of the 1 ML component (blue area), and (c) the doublet with 20% of the 1 ML component. The transfer integrals obtained are summarized in Table S1.

Table S1. Transfer integrals of the HOMO evaluated for 2ML films (in meV)

treatment	apparatus	model for fitting ^a			evaluated
		w/o 1 ML	10% 1-ML	20% 1-ML	
as-deposit ed	Chiba in 2014	91.5	94.5	97.0	94 ± 3
	Chiba in 2016	95.0	97.5	99.5	97 ± 2
	UVSOR-BL2B	91.5	93.0	98.5	95 ± 3
annealed	Chiba	101.5	105.5	108.5	105 ± 4

a) up to 20 % of the 1-ML component was incorporated as shown in Figure S5.

Table S2. Transfer integrals of the LUMO (in meV)

treatment	apparatus	model for fitting ^a			evaluated
		w/o 1 ML	10%-1 ML	20% 1-ML	
as-deposit ed	Chiba	121.5	124.5	128.5	124 ± 3
annealed	Chiba	128.0	132.0	136.0	132 ± 4

a) up to 20 % of the 1-ML component was incorporated as shown in Figure S5.

6. Effect of the energy resolution of the apparatus on the transfer integral

As mentioned in the main text (Experimental section), the energy resolutions of UPS and LEIPS are different and comparable to the determined transfer integrals. Here we show why the energy resolution of the apparatus does not affect the determined transfer integrals.

The observed spectrum h is a convolution of the true spectrum f which cannot be observed directly and the apparatus function g :

$$h = f * g. \quad (\text{S1})$$

When the spectrum of 2-ML f is expressed by the sum of the 1-ML spectra with different center energies f_i ($i = 1, 2$),

$$f = f_1 + f_2, \quad (\text{S2})$$

we practically observe the broadened spectrum,

$$h = (f_1 + f_2) * g. \quad (\text{S3})$$

In our data analysis, we decompose the observed spectrum h into the two components, h_1 and h_2 ,

$$h = h_1 + h_2. \quad (\text{S4})$$

From the linearity of the convolution, we get,

$$h = (f_1 + f_2) * g = f_1 * g + f_2 * g. \quad (\text{S5})$$

Here, $(f_i * g)$ stands for the broadened peak used in our analysis and is identical to h_i . Apparently, the peak positions are unchanged between $(f_i * g)$ and f_i for each of $i = 1$ and 2 . The above functions are visually expressed in Figure S6.

The above argument is easily extended to the analysis of the spectrum f from a film with n molecular layers, which is expressed by the sum of n 1-ML spectra with different center energies f_i ($i = 1 \dots n$),

$$f = \sum_i^n f_i. \quad (\text{S6})$$

In our data analysis, the spectrum h is decomposed into n -components, h_i ($i = 1 \dots n$),

$$h = \sum_i^n h_i. \quad (\text{S7})$$

From the linearity of deconvolution,

$$h = \sum_i^n h_i = \sum_i^n (f_i * g) = \left(\sum_i^n f_i \right) * g, \quad (\text{S8})$$

it follows that the peak energies are not affected by the apparatus function g .

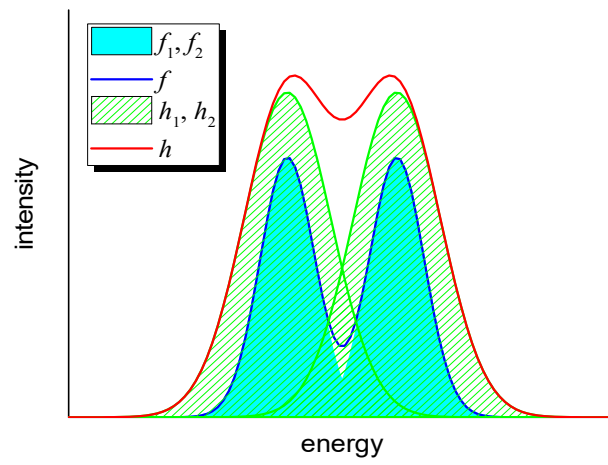


Figure S6. Relation between the true spectra f with the two components f_i and their convoluted (or broadened) function h with h_i . Note that the functions h and h_i correspond to the experimental spectrum and fitted curves, respectively (see the text for details).

References

1. Sojka, F.; Meissner, M.; Zwick, C.; Forker, R.; Fritz, T., Determination and Correction of Distortions and Systematic Errors in Low-Energy Electron Diffraction. *Rev. Sci. Instrum.* **2013**, *84*, 015111.